European Journal of Mechanics B/Fluids 52 (2015) 68–75

Contents lists available at ScienceDirect

European Journal of Mechanics B/Fluids

journal homepage: www.elsevier.com/locate/ejmflu

Practical mapping of the draw resonance instability in film casting of Newtonian fluids

M. Bechert [a,*], D.W. Schubert [a], B. Scheid [b]

[a] Institute of Polymer Materials, Friedrich–Alexander-Universität Erlangen-Nürnberg, Martensstr. 7, 91058 Erlangen, Germany

[b] TIPs, Université Libre de Bruxelles C.P. 165/67, 1050 Brussels, Belgium

HIGHLIGHTS

- The draw resonance effect in film casting is quantitatively analysed.
- A Newtonian model including inertia and gravity effects is used.
- Using fluidity and inlet velocity as dimensionless control parameters reveals non-monotonic stability behaviour.
- Various stability regimes are identified, including a regime of unconditional stability.
- Correlations between the critical draw ratio and the control parameters are given.

ARTICLE INFO

Article history:
Received 18 July 2014
Received in revised form
8 January 2015
Accepted 10 February 2015
Available online 23 February 2015

Keywords:
Draw resonance
Film casting
Stability map

ABSTRACT

The influence of viscosity and inlet velocity on the draw resonance instability of film casting processes is quantitatively analysed. By linear stability analysis of a Newtonian model including inertia and gravity effects, stability curves for different control parameter values are calculated numerically. For this purpose, we propose a scaling law which separates the fluidity, i.e. the reciprocal viscosity and the inlet velocity into two independent dimensionless parameters. This new scaling evidences a minimum of stability, separating two regimes of opposite behaviour: one for which increasing the inlet flow rate has a destabilizing effect due to viscosity and one for which increasing the inlet flow rate has a stabilizing effect due to gravity and inertia; increasing the fluidity has always a stabilizing effect. By fitting the stability curves with an appropriate postulated function, we are able to construct correlations between the critical draw ratio, the fluidity and the inlet velocity. For the first time regimes of negligible inertia or negligible gravity effects are revealed as well as a regime of unconditional stability. The proposed correlations for each of these regimes can further be used as an analytical solvable criterion for determining the onset of draw resonance in film casting.

1. Introduction

The process of film casting is of great importance in polymer and glass industry. In general, material, which is mostly in a molten state, is extruded through a slit die and drawn at higher speed, such that its thickness becomes thinner. Exceeding a critical take-up velocity, or equivalently exceeding the so-called critical draw ratio, oscillation in both flow velocity and width can be observed, which leads to minor quality of the end-product and eventually to the breakdown of the process. Miller [1] observed this phenomenon for the first time in fibre spinning and named it as draw resonance.

Since then, a lot of work has been done on the description of film casting processes, most of the studies focusing on the prediction of draw resonance, some including three-dimensional effects [2]. A comprehensive review is given in Chapter 10 of the book edited by Hatzikiriakos and Migler [3]. Yeow [4] has been the first who applied linear stability analysis on the process of isothermal film casting of a Newtonian fluid, neglecting all secondary forces like inertia, gravity, surface tension and air drag.

Shah and Pearson [5] investigated the effect of secondary forces on the stability of fibre spinning for the first time.[1] Newer results regarding the effect of inertia and gravity in film casting have been published by Cao et al. [6]. Using linear stability analysis, they investigated the dependence of the critical draw ratio and the oscillation frequency on Reynolds number *Re* and Froude number *Fr*. Moreover, a nonlinear analysis has been carried out in order to examine the influence of inertia and gravity on the oscillation amplitudes, film rupture and the time needed to reach sustained

* Corresponding author.
E-mail address: mathias.bechert@fau.de (M. Bechert).

[1] Besides a numerical factor, two-dimensional film casting and fibre spinning are mathematically equivalent, as will be also mentioned in Section 2.

http://dx.doi.org/10.1016/j.euromechflu.2015.02.005
0997-7546/

oscillation. One of their main conclusions is that both gravity and inertia effects improve stability, with inertia being the dominant force regarding stability. However, up to now a quantitative correlation between experimental processing parameters and the onset of instability is still missing. Cao et al. [6] considered a parameter range of Re $\in$ [0, 0.25] and Re/Fr $\in$ [0, 25]. This covers a wide practical range, but as presented here, it still misses experimental important parameter sets, including a regime where the instability vanishes completely.

Besides full numerical simulations some approximating methods have been developed, which greatly facilitates the computation of the critical draw ratio with respect to the system parameters. One of such alternative approaches is Hyun's stability criterion [7], later adapted by Kim et al. [8], which correlates the cycle time of draw resonance with the travelling time of a mass element through the system. Hagen published several mathematical analysis on draw resonance, including some works on the asymptotic behaviour of the eigenvalue spectrum of the linearised solutions for both isothermal [9] and non-isothermal [10] models. Moreover, Van der Hout [11] derived another stability criterion for fibre spinning of Newtonian and power law fluids. However, to our knowledge no correlations between the critical draw ratio and process and material parameters including the effects of inertia and gravity have been revealed yet.

In our work, the inlet velocity and the fluidity, i.e. the reciprocal viscosity, are used as control parameters as it is the case in practical settings. We start with a short presentation of the common model equations and introduce a scaling rule which facilitates the examination of the influence of the control parameters on the onset of the instability. This is followed by a description of the stability analysis method, including the postulation of an analytical solvable expression for the stability curves, which can be fitted to the numerical data and used as an estimator for the critical draw ratio. As a result, we can identify regimes where gravity, or inertia respectively, can be neglected, as well as a regime of unconditional stability. These are all summarised in a stability map covering the practical range of the control parameters. The paper closes with conclusions and outlook.

2. Model equations and scaling

We follow the usual procedure of modelling the film casting process for stability analysis, as presented for example by Cao et al. [6]. Fig. 1 shows the three-dimensional sketch of a film which is drawn along the x-axis over a total distance L. In this work a one-dimensional model is used, using the assumption of infinite width. Under the assumption that the film thickness $h(x, t)$ is small compared to L, i.e. $h/L \ll 1$, the flow velocity in x direction, denoted by u, does not change across the thickness at leading order, i.e. $u = u(x, t)$, t being the time. The continuity equation can then be written,

$$\partial_t h + \partial_x(hu) = 0. \tag{1}$$

Following Yeow [4], we use a Newtonian constitutive equation. The momentum balance equation then has the following form, neglecting surface tension and air drag[2]:

$$\rho h\,(\partial_t u + u\partial_x u) = \partial_x\,(4h\eta\partial_x u) + g\rho h, \tag{2}$$

where the left-hand side accounts for inertia and the two terms on the right-hand side account, respectively, for viscous stresses and gravity; ρ and η are, respectively, the density and the dynamical

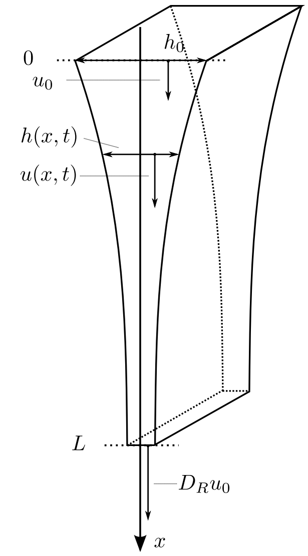

Fig. 1. Sketch of film casting process.

viscosity of the material, both assumed to be constant, and g is the acceleration of gravity. The factor 4 in Eq. (2) is the so-called 'Trouton ratio'.

Within the process of film casting, material is extruded with a certain velocity u_0 through a slit die of thickness h_0 and taken up by a chill roll rotating with predefined speed. This sets the boundary conditions, which are

$$u(0, t) = u_0, \qquad u(L, t) = D_R u_0, \qquad h(0, t) = h_0, \tag{3}$$

where D_R is the so-called draw ratio, strictly larger than unity.

In this work, we are considering that the length L is fixed and that the adjustable control parameters, in addition to the draw ratio, are the inlet velocity and the viscosity. The former can be changed by different extrusion dies or different flow rates, the latter by modifying the temperature or the material itself. In order to get dimensionless variables, we are therefore using the following transformation rules:

$$x \to Lx, \qquad u \to \sqrt{gL}\,u, \qquad h \to h_0 h, \qquad t \to \sqrt{\frac{L}{g}}\,t. \tag{4}$$

Applying the transformations (4) to (1) and (2) leads to the following system:

$$\partial_t h + \partial_x(hu) = 0, \tag{5a}$$

$$Fh(\partial_t u + u\partial_x u - 1) - \partial_x(h\partial_x u) = 0, \tag{5b}$$

where $F = \frac{\sqrt{gL^3}\rho}{4\eta}$ is the fluidity parameter, i.e. the dimensionless reciprocal viscosity. The boundary conditions in (3) become

$$u(0, t) = Q, \qquad u(L, t) = D_R Q, \qquad h(0, t) = 1, \tag{6}$$

where $Q = \frac{u_0}{\sqrt{gL}}$ is the dimensionless inlet velocity. The pure viscous model reported in [4] is recovered by setting $F = 0$, for any $Q \neq 0$; for convenience, we have set $Q = 1$. It is worth mentioning that all the equations mentioned here can merely be transferred to the fibre spinning model first proposed by Matovich and Pearson [12] by substituting the thickness $h(x, t)$ with the cross-sectional area of the fibre and additionally changing the Trouton ratio 4, which appears in F, to 3. Nevertheless, surface tension effects induced by transverse curvature variations along the fibre have to be considered in addition to gravity and inertia.

Notice that the velocity scale $\sqrt{gL}$ is the characteristic velocity of a fluid particle falling along the length L under gravity. For a

[2] As indicated by a referee, these assumptions may be inappropriate for modelling of fibre spinning, limiting the comparability of these results with the fibre spinning process.

Table 1
Practical ranges of the process parameters and resulting ranges of the dimensionless parameters. Note that although the length L may vary for different applications, it is assumed to be constant for a particular process.

Parameter	Unit	Range
L	m	10^{-2}–1
η/ρ	$m^2\ s^{-1}$	10^{-1}–10^2
u_0	ms^{-1}	10^{-3}–1
Q	1	10^{-4}–1
F	1	10^{-5}–10

film of fixed length, this velocity is fixed, hence independent of the control parameters, which is the aim of this scaling. Having used the inlet velocity u_0 as a scale, instead, as usual in the literature, would have lead to similar equations but expressed in terms of the Reynolds number $Re = \frac{\rho u_0 L}{4\eta}$ and the Froude number $Fr = \frac{u_0^2}{gL}$. In our scaling, the velocity u_0 only appears in the parameter Q. The correspondence between the two scalings is straightforward, but nonlinear, namely $Re = QF$ and $Fr = Q^2$. Table 1 shows all parameter regimes, which have practical importance, and the resulting ranges of F and Q.[3]

3. Stability analysis

In order to examine the stability of the process, we apply the standard tools of linear stability analysis and use the following ansatz:

$$u(x,t) = u_s(x)(1 + U(x)e^{\lambda t}), \tag{7a}$$

$$h(x,t) = h_s(x)(1 + H(x)e^{\lambda t}), \tag{7b}$$

where $u_s(x)$ and $h_s(x)$ represent the steady state solutions, $U(x)$ and $H(x)$ the spatial modes of the perturbations and λ the eigenvalues.

Looking for the base state first by neglecting the time derivatives, Eq. (5a) leads together with the boundary conditions (6) to

$$h_s = \frac{Q}{u_s}, \tag{8}$$

while Eq. (5b) becomes

$$u_s'' = F\left(u_s u_s' - 1\right) - \frac{h_s' u_s'}{h_s}, \tag{9}$$

where the prime denotes the derivative with respect to x. The evolution equations for the perturbations are gained by substitution of (7) into (5) and rearranged by using the steady state Eqs. (8) and (9):

$$H' = -\left(\frac{H h_s \lambda}{Q} + U'\right), \tag{10a}$$

$$U'' = \frac{1}{Q h_s}\left[h_s Q F U(\lambda + u_s') + Q U'(-h_s' + QF) + h_s^2\left(FU - u_s'(H' + 2U')\right)\right]. \tag{10b}$$

In order to compute the neutral stability curves, which separate the parameter space in stable and unstable regimes, we use the method presented by Scheid et al. [13]. According to linear stability theory, the steady states are unstable if there exists at least one eigenvalue λ with $\text{Re}(\lambda) > 0$, otherwise they are stable.

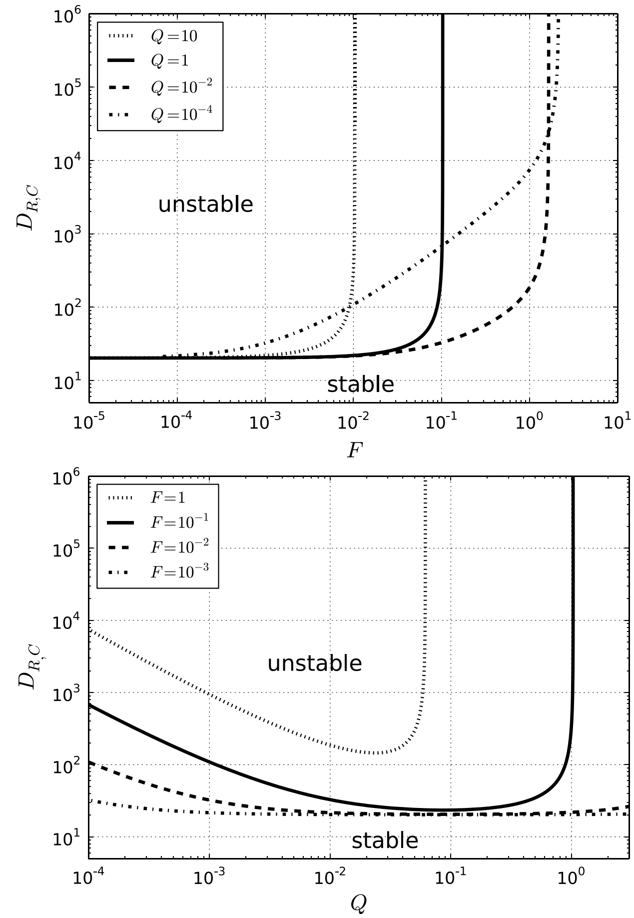

Fig. 2. Stability curves for various values of the dimensionless inlet velocity Q (top) and various values of the dimensionless fluidity F (bottom).

Table 2
Comparison of calculated $D_{R,C}$ and $\text{Im}(\lambda)$ for some values of F and Q with the corresponding solutions presented by Cao et al. [6].

Process parameters		This work		Cao et al. [6]	
F	Q	$D_{R,C}$	$\text{Im}(\lambda)$	$D_{R,C}$	$\text{Im}(\lambda)$
0	1	20.218	14.011	20.218	14.011
0.25	0.1	30.343	1.5895	30.343	1.5895
0.5	0.1	56.273	1.7732	56.267	1.7731

Therefore we need to find solutions having a spectrum of eigenvalues with the largest real part being zero. Neglecting inertia and gravity forces, i.e. $F \to 0$, there exists an analytical solution for Eqs. (8)–(10) [14,15], even though various authors [4,16,17] found it first numerically, which leads to a critical draw ratio of $D_{R,C} = 20.218$ and a dimensionless pulsation of $\text{Im}(\lambda) = 14.01$. Starting from this known solution, a continuation method is used via the software AUTO-07P [18] to obtain solutions and track $D_{R,C}$ for arbitrary values of fluidity F and inlet velocity Q. A comparison with the values calculated by Cao et al. [6] in Table 2 shows excellent agreement. For all parameter combinations which have been analysed in this work, we have computed the solutions up to values of $D_{R,C}$ of at least 10^6. This definitely covers all practical relevant regimes for drawing processes.

Fig. 2 shows some of the computed stability curves for constant values of Q and F, respectively. From a qualitative point of view it can be stated, on basis of the curves with constant Q, that the system becomes unconditionally stable if the fluidity F is larger than a certain threshold value. This threshold depends on Q, e.g. for $Q = 1$ it is approximately 10^{-1} and grows with decreasing Q. Additionally, the curves start earlier to raise with decreasing

[3] Some parameter combinations within these ranges are more exotic than others, such as for instance small length ($\sim 10^{-2}$ m) and large inlet velocity (~ 1 m/s). However, for reasons of completeness we do not introduce further constraints here.

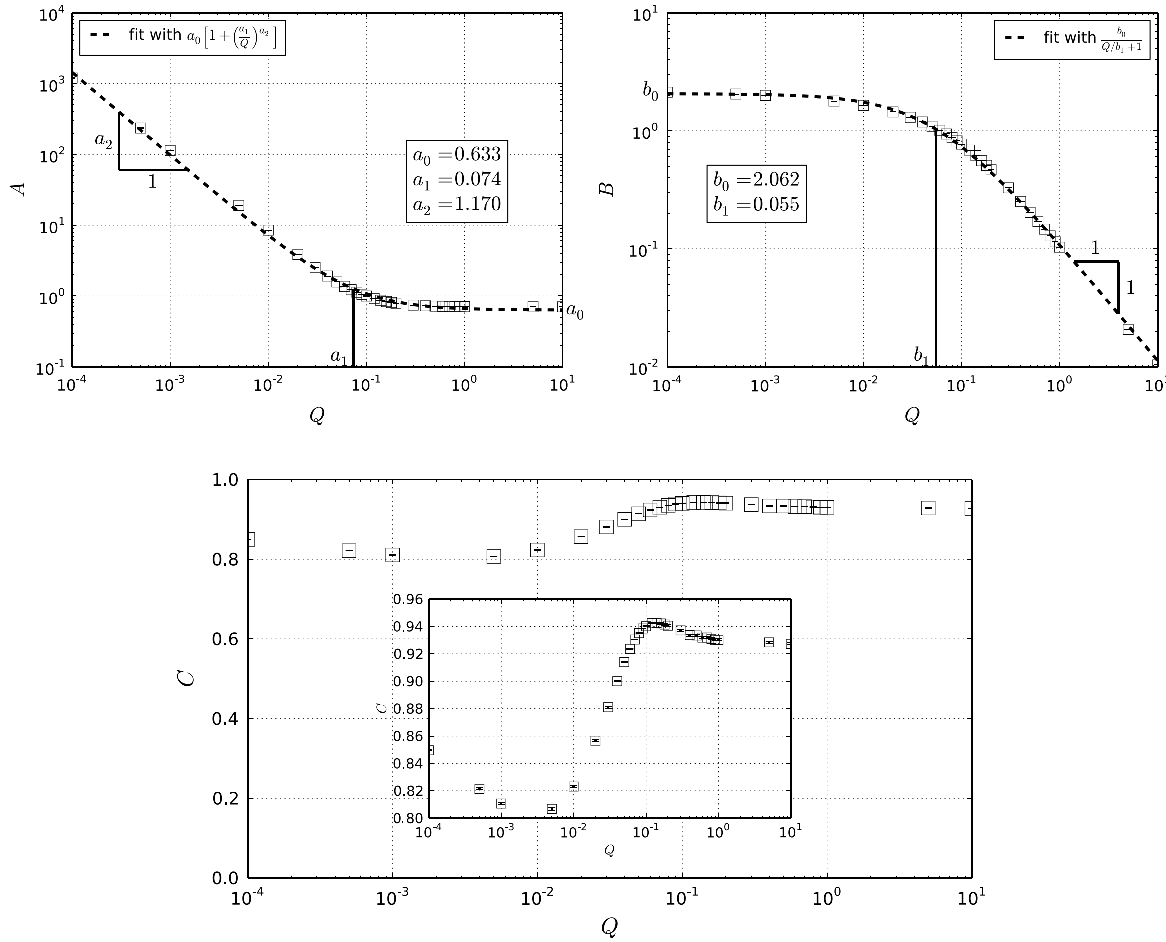

Fig. 3. Fitting parameters A, B and C from the correlation function (11) for several values of Q.

Q, which can be seen especially for $Q = 10^{-4}$. The curves for constant values of F show distinct behaviour for low and high values of Q. While the critical draw ratio decreases with increasing Q if Q itself is small, it increases with increasing Q for large Q. In other words two distinct regimes exist, one for which increasing the inlet velocity has a destabilising effect and one for which it has a stabilising effect. Between these two regimes, a minimum of stability occurs. This minimum increases with F, depicting again the stabilising effect of fluidity. For values of F which are large enough, the regime of unconditional stability appears as well in the practical range of Q.

Our goal is to achieve a quantitative analysis of the stability behaviour with respect to the dimensionless parameters F and Q. For this purpose, we postulate an empirical function which can be fitted to the numerically calculated curves for constant Q, as they have a simpler shape compared to the curves with constant F. The fit function itself is defined in the following way:

$$D_{R,C} = f(F; A, B, C) := 20.218\left[1+\left(\frac{AF}{B-F}\right)^{C}\right], \tag{11}$$

with fitting parameters A, B and C. Analysing these fitting parameters, which quantify characteristic properties of the curves with respect to Q, will then lead to deeper insight in the influence of both F and Q on the draw resonance behaviour.

The choice of the correlation function (11) is explained in the following. As already mentioned above, the viscous limit of $D_{R,C} = 20.218$ is reached for $F \to 0$. Therefore this value appears explicitly in (11) in order to fulfil this condition by default. For the description of the divergency, the simplest function type showing divergent behaviour, i.e. $f(x) \propto \frac{1}{x}$, has been chosen. So parameter B corresponds to the threshold value of F for unconditional stability. It has to be mentioned that we do not prove the divergence of the numerical data rigorously. However, the critical draw ratio has been calculated for all practical relevant values and therefore, it is reasonable to assume a divergent behaviour here as inferred from Fig. 2. The numerator AF accounts for the fact that the curves have different steepness for different Q. The exponent C has been added for technical reasons, as it makes a fine tuning of the slope possible, but it appears to remain close to unity for all Q.

The fitting is performed using the Python package SCIPY.ODR, which is an interface to the FORTRAN-77 library ODRPACK. This algorithm is based on the so-called Deming regression [19], which is explained in detail in Appendix.

The motivation of the quantitative analysis lies in the advantage of being able to calculate adequate processing windows easily. We shall give a simple example for that. In a typical film casting process, the thickness of the final product is prescribed to be below a certain value, or alternatively the draw ratio has to be above a certain value. If the material is prescribed as well, the fluidity is fixed, at least to a small interval. If a correlation like (11) is known, it is possible to directly calculate values for the inlet velocity which allow stable processing.

4. Results

A various number of curves for values of the inlet velocity Q between 10^{-4} and 10 have been analysed, in accordance with the range of practical values (cf. Table 1). Fig. 3 shows the dependencies of the fitting parameters A, B and C on Q.

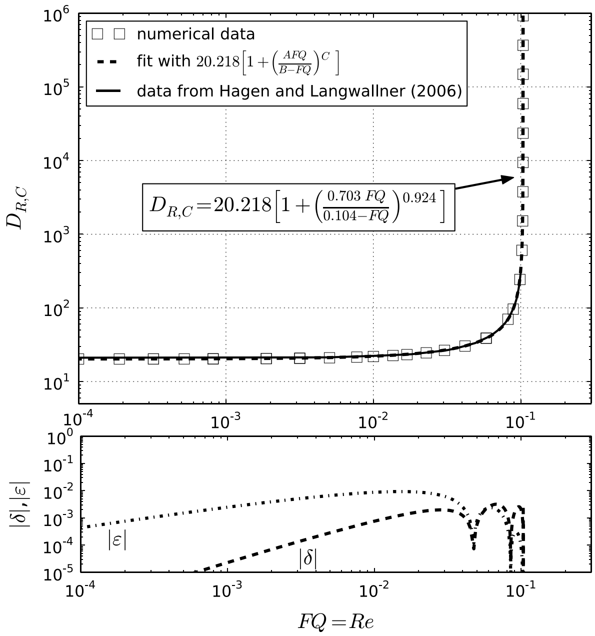

Fig. 4. Stability diagram for the 'viscous–inertia' model, i.e. neglecting gravity effect, together with a fit function. The deviations δ and ε in both variables show the accuracy of the fit and are explained in Appendix. Only few points of the numerical data are shown for the sake of readability. Additionally, the curve presented by Hagen and Langwallner [20] is drawn for comparison purpose.

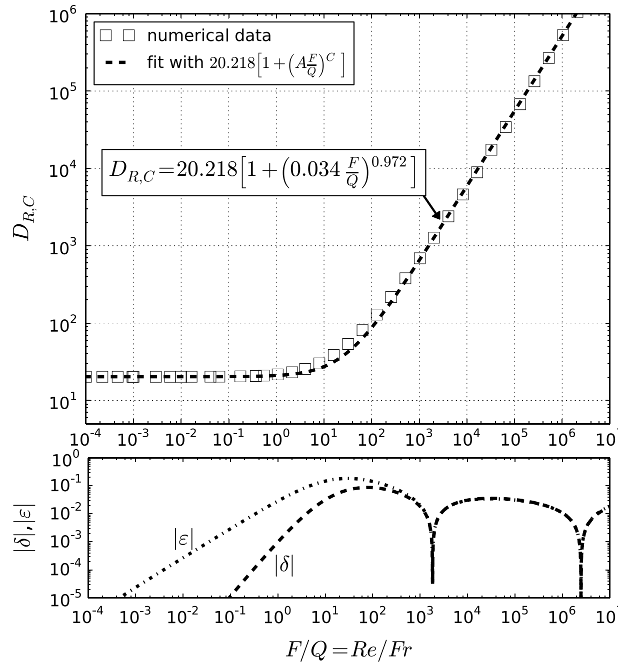

Fig. 5. Stability diagram for the 'viscous–gravity' model, i.e. neglecting inertia effect, together with a fit function. The deviations δ and ε in both variables show the accuracy of the fit and are explained in Appendix. Only few points of the numerical data are shown for the sake of readability.

It is possible to fit parameters A and B with the following functions:

$$A(Q) := a_0\left[1+\left(\frac{a_1}{Q}\right)^{a_2}\right], \tag{12a}$$

$$B(Q) := \frac{b_0}{Q/b_1+1}, \tag{12b}$$

as shown in Fig. 3. We will concentrate on these two parameters first. Parameter C varies only in a small range and will not be included in the first part of the analysis, ignoring the small discrepancies in the various fitting results.

Both parameters A and B show two qualitative distinct regimes for small and large values of Q, as qualitatively identified in Fig. 2. According to the fitting parameters a_1 and b_1 shown in Fig. 3, the transition from one regime to the other appears at about $Q \approx 0.06$. In the following, each regime is analysed separately.

4.1. $Q \gg 0.06$ and 'viscous–inertia' model

Regarding only large values of Q, or more precisely regarding the region of $Q \gg a_1, b_1$, we get the following limit behaviour:

$$A(Q) \approx a_0, \tag{13a}$$

$$B(Q) \approx \frac{b_0 b_1}{Q}. \tag{13b}$$

Inserting (13) into (11) gives

$$D_{R,C} \approx 20.218\left[1+\left(\frac{a_0 FQ}{b_0 b_1 - FQ}\right)^C\right]. \tag{14}$$

Eq. (14) shows a dependency of $D_{R,C}$ only on the product FQ, which means that all curves in this region can be mastered by one single curve. As FQ is identical to the Reynolds number Re, it is possible to directly compare this master curve with the stability curve of a model considering only viscous and inertia forces and neglecting gravity, which corresponds to dropping the third term in the momentum balance equation (5b). Fig. 4 shows the stability curve for this 'viscous–inertia' model.

It was fitted with the function resulting from substituting F with FQ into (11). The fitting parameters shown in Fig. 4 are in good agreement with the corresponding parameters in (14), i.e. a_0 and $b_0 b_1$. This shows that, regarding the stability, gravity effect can be neglected in comparison to inertia effect, if the inlet velocity is above a certain threshold value.

It is worth mentioning that this divergent behaviour can also be seen in the figures given by Shah and Pearson [5] and Hagen and Langwallner [20]. The result of the latter is plotted in Fig. 4 that shows perfect coincidence with our curve, including the threshold value for FQ, $b_0 b_1 = 0.11$.

4.2. $Q \ll 0.06$ and 'viscous–gravity' model

If only small values of Q, i.e. $Q \ll a_1, b_1$, are taken into account, Eqs. (12) simplify to

$$A(Q) \approx a_0\left(\frac{a_1}{Q}\right)^{a_2}, \tag{15a}$$

$$B(Q) \approx b_0. \tag{15b}$$

If we further approximate $a_2 \approx 1$, (11) can be written as

$$D_{R,C} \approx 20.218\left[1+\left(\frac{a_0 a_1 (F/Q)}{b_0 - F}\right)^C\right]. \tag{16}$$

In contrast to Eq. (14), this expression cannot directly be mastered by one single curve. If $F \ll b_0$, however, the denominator in (16) can be approximated by b_0, resulting in an expression which only depends on F/Q. The resulting error of neglecting the denominator is smaller than 10% if $F < 0.2$. For this region, we can compare the curve with the stability analysis of a model including only viscous and gravity effects, as F/Q is equivalent to Re/Fr, which compares gravity and viscous forces. Such an analysis can be achieved by neglecting the first two terms in (5b). Fig. 5 visualises

Table 3
Correlations between the critical draw ratio and the control parameters F and Q, dependent on the different regimes visualised in Fig. 6(a). The expressions of $A(Q)$ and $B(Q)$ are given in (12), while $C(Q)$ should be inferred from Fig. 3.

Label	Regime	$D_{R,C}/20.218$
I	Viscous	1
II	Viscous–gravity	$1+\left(0.034\frac{F}{Q}\right)^{0.972}$
III	Viscous–inertia	$1+\left(\frac{0.703FQ}{0.104-FQ}\right)^{0.924}$
IVa	Viscous–gravity–inertia	$1+\left(\frac{0.0468F/Q}{2.062-F}\right)^{C(Q)}$
IVb	Viscous–gravity–inertia	$1+\left(\frac{A(Q)F}{B(Q)-F}\right)^{0.94}$
V	unconditionally stable	–

this 'viscous–gravity' model. The fit function can be obtained from (11) by replacing F with F/Q and omitting the denominator. Again, the fitting parameter A of the 'viscous–gravity' model matches to the limit value a_0a_1/b_0, indicating that within this particular region inertia effect is negligible and only viscous and gravity effects are responsible of the stability behaviour.

4.3. Regimes and stability maps

Eqs. (11), (14) and (16) show that the critical draw ratio can be seen as a superposition of the result of the viscous model, i.e. $D_{R,C} = 20.218$, and a term describing the inertia and/or gravity effects, tuned by the control parameters F and Q. Therefore there exist parameter combinations which lead to negligible small contributions of both inertia and gravity effects, resulting in a pure viscous regime. The area of this regime has been determined arbitrarily by restricting $20.218 < D_{R,C} < 21$, i.e. a variation of less than 4% of the critical draw ratio as compared to the viscous model.

Together with the results of the viscous-gravity and viscous-inertia models described above it is possible to reveal regimes in the parameter space (F, Q), where either viscous or viscous and gravity or viscous and inertia effects have the most influence on stability. Fig. 6(a) visualises these regimes together with Table 3. The threshold values for Q limiting regime IVb have been obtained by fitting constant or reciprocal, respectively, functions to the corresponding regimes of $A(Q)$ and $B(Q)$ and determining the values of Q, where the deviation from the numerical data is larger than 10%. It is remarkable that inertia effect is always dominant if the inlet velocity Q is large enough, whereas it can be neglected for small Q only if the fluidity F is below 0.2. This asymmetry can also be observed in the evolution of parameter C in Fig. 3. For large Q, the value of 0.924 of the 'viscous–inertia' regime is approached. In contrast to that, for low Q no trend to a limit value for C can be observed, as the divergence of the stability curves does not vanish like it does for the 'viscous–gravity' model. In the region around $Q \approx 0.06$, the value of C can be approximated by 0.94.

In Table 3, corresponding correlations between the critical draw ratio $D_{R,C}$ and the control parameters F and Q are given for the various regimes as well. In the 'viscous–gravity–inertia' regime IVa, i.e. for $Q \ll 0.06$, parameter C has to be estimated directly from Fig. 3. For the 'viscous–gravity–inertia' regime IVb, the expressions for A and B given in (12) have to be used, with the numerical values of the correlation constants given in Fig. 3.

Fig. 6(b) shows a stability map for the control parameters F and Q. The dashed lines indicate parameter combinations where the critical draw ratio $D_{R,C}$ is constant. In between two of those curves, $D_{R,C}$ shows monotonical behaviour. For materials with low fluidity F, $D_{R,C}$ is more or less constant, as viscous effects are dominant. Especially in the transition region around $Q \approx 0.06$, the stability of the system does not change notably within more than two orders of magnitude in F. On the other hand, for sufficiently large F the instability disappears, no matter which value the inlet velocity has. The threshold value, i.e. parameter B of (11), decreases with increasing Q, which means that for high inlet velocities, materials with $F \approx 0.1$ may already show unconditionally stable behaviour.

The region underneath the grey dotted lines in Fig. 6(b) corresponds to the parameter sets covered by the analysis of Cao et al. [6]. To our knowledge, this is the first time that a regime of unconditional stability is revealed and correlated with process parameters. A three-dimensional visualisation of the stability map can be seen in Fig. 6(c).

One of the results of Shah and Pearson [5] and Cao et al. [6] is that while both inertia and gravity enhance stability, gravity shows a rather weak influence in comparison to inertia. However, our results show that a comparison of both forces is more subtle. For $Q \ll 0.06$ and $F < 0.01$, which belongs to the 'viscous–gravity' regime, $D_{R,C}$ increases faster with increasing fluidity as it does for $Q \gg 0.06$, i.e. in the 'viscous–inertia' regime.

4.4. Stabilising mechanism of gravity and inertia

Note that the transition to the regime of unconditional stability can be described in terms of the Reynolds number $Re = FQ$ only for large values of Q, as it has been shown above. If Q is small, a constant value of F indicates the divergence of $D_{R,C}$. This reveals that although the effect of unconditional stability is caused by inertia effect, the onset point can be altered by gravity. A possible explanation for this stabilising effect of gravity has been given by Schultz and Davis [14], who stated that a constant force along the streamline enhances stability. They describe the mechanism of draw resonance by perturbation waves travelling from the inlet to the chill roll, where they are reflected back upstream. If the force at the chill roll is fixed instead of a prescribed outlet velocity, the waves can only travel downwards, preventing an onset of draw resonance. If the boundary condition at the chill roll is a combination of prescribed velocity and force, the waves are partially reflected. Depending on the degree of reflection, the perturbations are amplified or not. Thus, a constant force like gravity hinders the waves to be reflected at the chill roll, leading to higher stability. Similarly, high inertia forces damp down the force perturbations near the chill roll and increase the critical draw ratio. In the present work, we observed that there exists a critical Reynolds number, beyond which no instability exists for all values of draw ratio. In the picture of the stability mechanism this implies that nothing of the downward perturbation wave is reflected at the chill roll if inertia forces are beyond a finite threshold value. Unfortunately, we do not have a comprehensive explanation for this phenomenon yet and leave it open to future work.

5. Conclusions and outlook

We have investigated the influence of the dimensionless inlet velocity Q and fluidity F on the onset of draw resonance in film casting processes including gravity and inertia effects. For this purpose, stability curves with F as independent parameter have been computed numerically for various values of Q using a continuation method. These curves have been fitted with an appropriately postulated function with three fitting parameters, one of which representing a threshold value of F beyond which the system is unconditionally stable. Correlations between these parameters and Q have been revealed, discussed and quantified. With respect to F and Q, we could identify a regime where viscous and inertia effects are dominant and gravity effect can be neglected, as well as a regime where viscous and gravity effects are dominant and inertia effect can be neglected. For the first time, we revealed a regime of unconditional stability, which shows up for materials with rather high fluidity and which is caused by inertia effects. The mechanism behind this effect is not completely understood yet. Besides a stability map which visualises the stability behaviour of the system

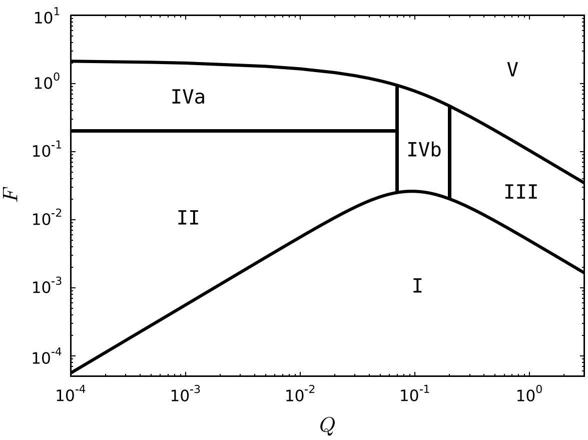

(a) Visualisation of different regimes in the control parameter space. The labels are explained in Table 3, together with corresponding correlations between the critical draw ratio and parameters F and Q.

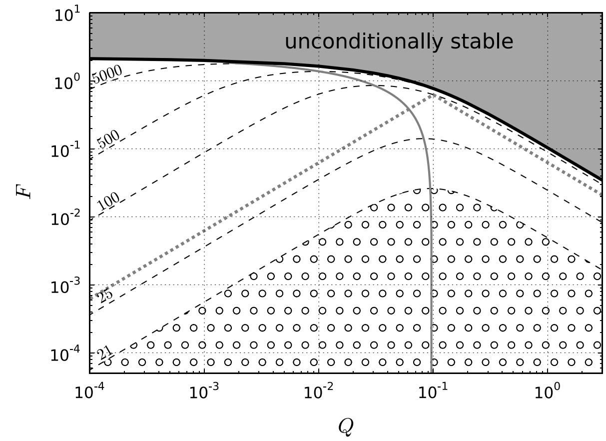

(b) Stability map with control parameters F and Q. The dashed lines belong to parameter sets with a constant critical draw ratio $D_{R,C}$ of 21, 25, 100, 500 and 5000. The dark shaded area marks the region where no draw resonance occurs due to inertia effect. In the dotted region, the critical draw ratio is between 20.218 and 21, i.e. the viscous regime. The solid grey line in the middle separates the regime where increasing Q is stabilising from the regime where increasing Q is destabilising for constant F. The region underneath the grey dotted lines encompasses the parameter range covered by Cao et al. [6].

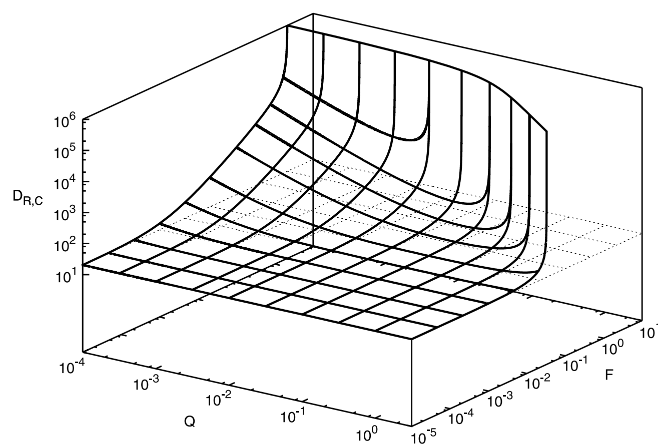

(c) Three-dimensional visualisation of the stability map with control parameters F and Q.

Fig. 6. Results of the stability analysis. Plots (a) and (b) are complementary and need to be considered together.

with respect to the control parameters, we showed an analytical solvable criterion for the critical draw ratio which enables a quick and highly accurate determination of stable processing conditions.

The model presented in this paper neglects several effects which are known to be crucial for the stability of the process, e.g. thermal cooling or non-Newtonian material effects. However, we believe that the presented method can be extended to cover the most important effects necessary to provide a predictive tool for practical use. To realise this, supporting experimental investigations are mandatory to be able to carve out the essential model assumptions. We hope to approach this goal further in forthcoming work.

Acknowledgements

M.B. would like to thank M.Sc. Michael Härth, M.Sc. Johannes Krückel and M.Sc. Peter Kunzelmann for fruitful discussions. B.S. acknowledges the F.R.S.—FNRS for financial support, as well as the IAP 7/38 MICROMAST program initiated by BELSPO (no. IAP-7/38).

Appendix. Deming regression

The method of Deming regression [19] is similar to the method of least squares but with the additional possibility of considering variances of the independent variable. In other words, χ, defined by

$$\chi := \sum_{i=1}^{n} \left[w_{\tilde{\varepsilon}_i}^2 \tilde{\varepsilon}_i^{\,2} + w_{\tilde{\delta}_i}^2 \tilde{\delta}_i^{\,2} \right], \tag{A.1a}$$

$$\text{with} \quad \tilde{\varepsilon}_i = f\left(F_i + \delta_i; A, B, C\right) - D_{R,C;i}, \tag{A.1b}$$

is minimised. The index i enumerates the data points, whose total number is n; $\tilde{\delta}_i$ is the deviation from each point F_i and $w_{\tilde{\varepsilon}_i}$ and $w_{\tilde{\delta}_i}$ are the weights for the deviations. The minimum is searched for a set of both (A, B, C) and the set of $\tilde{\delta}_i$. If $\tilde{\delta}_i \to 0$ for all i, the common least squares method is obtained. We are using this extended method because of the divergent character of the data. A small shift of the fit function in horizontal direction near the threshold point leads to a high change in the residual sum of squares because of the high gradient in this region. This has the effect that the parameters are mostly fitted to a small interval of data points, having larger residuals for the rest. Allowing uncertainty also in F reduces the accuracy of the threshold value but improves the coincidence of numerical data and fit function in total (see Fig. A.7). As weights $w_{\tilde{\varepsilon}_i}$ and $w_{\tilde{\delta}_i}$, the reciprocal values of $D_{R,C;i}$ and F_i are used so that the relative error is minimised. In this work, we use the relative

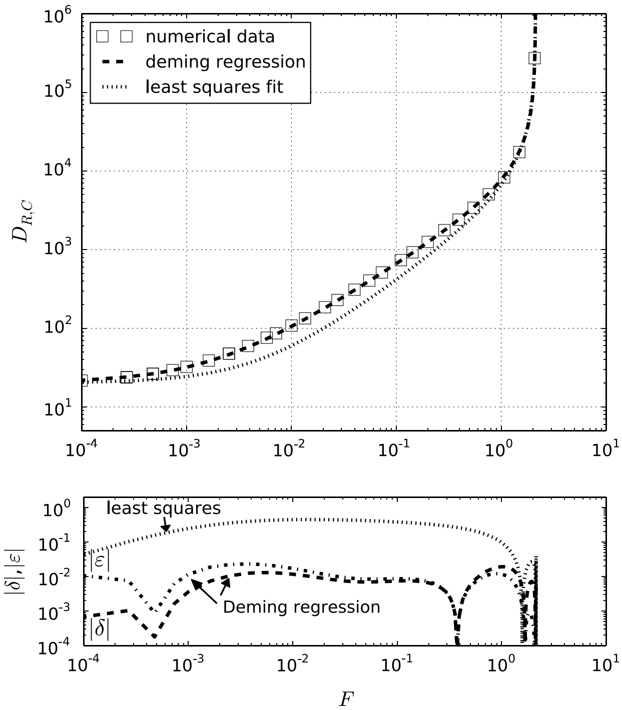

Fig. A.7. Comparison of deming regression and method of least squares. Only few points of the numerical data are shown for the sake of of readability.

error values

$$\delta := w_{\tilde{\delta}}\tilde{\delta}, \qquad \varepsilon := w_{\tilde{\varepsilon}}\tilde{\varepsilon}. \tag{A.2a}$$

Fig. A.7 also shows the absolute value of δ and ε for both fit methods, which makes a quantitative comparison possible. Moreover, it can be seen that the correlation function in (11) seems to be appropriate to describe the stability curves, as the error in both variables $D_{R,C}$ and F is only 1%–2% maximum.

References

[1] J.C. Miller, Swelling behavior in extrusion, Polym. Eng. Sci. 3 (2) (1963) 134–137.
[2] B. Scheid, S. Quiligotti, B. Tran, H.A. Stone, Lateral shaping and stability of a stretching viscous sheet, Eur. Phys. J. B 68 (4) (2009) 487–494.
[3] S. Hatzikiriakos, K. Migler (Eds.), Polymer Processing Instabilities: Understanding and Control, Marcel Dekker, New York, 2005.
[4] Y.L. Yeow, On the stability of extending films: a model for the film casting process, J. Fluid Mech. 66 (3) (1974) 613–622.
[5] Y.T. Shah, J.R.A. Pearson, On the stability of nonisothermal fiber spinning-general case, Ind. Eng. Chem. Fundam. 11 (2) (1972) 150–153.
[6] F. Cao, R.E. Khayat, J. Puskas, Effect of inertia and gravity on the draw resonance in high-speed film casting of Newtonian fluids, Internat. J. Solids Structures 42 (21–22) (2005) 5734–5757.
[7] J.C. Hyun, Theory of draw resonance: part I. Newtonian fluids, AIChE J. 24 (3) (1978) 418–422.
[8] B.M. Kim, J.C. Hyun, J.S. Oh, S.J. Lee, Kinematic waves in the isothermal melt spinning of Newtonian fluids, AIChE J. 42 (11) (1996) 3164–3169.
[9] T. Hagen, Eigenvalue asymptotics in isothermal forced elongation, J. Math. Anal. Appl. 244 (2) (2000) 393–407.
[10] T. Hagen, M. Renardy, Eigenvalue asymptotics in non-isothermal elongational flow, J. Math. Anal. Appl. 252 (1) (2000) 431–443.
[11] R. Van der Hout, Draw resonance in isothermal fibre spinning of Newtonian and power-law fluids, European J. Appl. Math. 11 (2) (2000) 129–136.
[12] M.A. Matovich, J.R.A. Pearson, Spinning a molten threadline. Steady-state isothermal viscous flows, Ind. Eng. Chem. Fundam. 8 (3) (1969) 512–520.
[13] B. Scheid, S. Quiligotti, B. Tran, R. Gy, H.A. Stone, On the (de)stabilization of draw resonance due to cooling, J. Fluid Mech. 636 (2009) 155–176.
[14] W.W. Schultz, S.H. Davis, Effects of boundary conditions on the stability of slender viscous fibers, J. Appl. Mech. 51 (1) (1984) 1–5.
[15] M. Renardy, Draw resonance revisited, SIAM J. Appl. Math. 66 (4) (2006) 1261–1269.
[16] J.R.A. Pearson, M.A. Matovich, Spinning a molten threadline: stability, Ind. Eng. Chem. Fundam. 8 (4) (1969) 605–609.
[17] D. Gelder, The stability of fiber drawing processes, Ind. Eng. Chem. Fundam. 10 (3) (1971) 534–535.
[18] E. Doedel, A. Champneys, T. Fairgrieve, Y. Kuznetsov, B. Sandstede, X. Wang, AUTO97 continuation and bifurcation software for ordinary differential equations, 1997. AUTO software is freely distributed on http://indy.cs.concordia.ca/auto/.
[19] W.E. Deming, Statistical Adjustment of Data, Dover Publ., New York, 1964.
[20] T. Hagen, B. Langwallner, A numerical study on the suppression of draw resonance by inertia, ZAMM Z. Angew. Math. Mech. 86 (1) (2006) 63–70.